Two-Photon Induced Blue Shift of Core and Shell Optical Transitions in Colloidal CdSe/CdS quasi-type II Quantum Rods

Marco Allione,[1] Ana Ballester,[2] Hongbo Li,[1] Alberto Comin,[1] José L. Movilla,[2,#] Juan I. Climente,[2] Liberato Manna[1] and Iwan Moreels[1,*]

1 Istituto Italiano di Tecnologia, Via Morego 30, IT-16163 Genova, Italy

2 Departament de Quimica Fisica i Analitica, Universitat Jaume I, E-12080 Castellón, Spain

*iwan.moreels@iit.it, #movilla@qfa.uji.es

Abstract

The spectral dependence of the two-photon absorption in CdSe/CdS core/shell nanocrystal heterorods has been studied via two-photon induced luminescence excitation spectroscopy. We verified that the two-photon absorption in these samples is a purely nonlinear phenomenon, excluding the contribution from multi-step linear absorption mediated by defect states. A large absorption cross section was observed for CdSe/CdS core/shell quantum rods, in the range of 10^5 GM (1 GM = 10^{-50} cm^4 sec phot^{-1}), scaling with the total nanocrystal volume and thus independent of the core emission wavelength. In the two-photon luminescence excitation spectra, peaks are strongly blue-shifted with respect to the one-photon absorption peaks, for both core and shell transitions. The experimental results are confirmed by *k.p* calculations, which attribute the shift to both different parity selection rules that apply to one-photon and two-photon transitions, and a low oscillator strength for two-photon transitions close to the ground state one-photon absorption. In contrast with lead chalcogenide quantum dots, we find no evidence of a breakdown of the optical selection rules, despite the presence of band anisotropy, *via* the anisotropic hole masses, and the explicitly induced reduction of the electron wavefunction symmetry *via* the rod shape of the shell. The anisotropy does lead to an

unexpected splitting of the electron *P*-states in the case of a large CdSe core encapsulated in a thin CdS shell. Hence, tuning of the core and shell dimensions, and the concurring transition from type-I to quasi type-II carrier localization, enables unprecedented control over the band-edge two-photon absorption.

MAIN TEXT

Colloidal semiconductor nanocrystals, currently synthesized in various forms such as quantum dots (Qdots), quantum rods (Qrods), and more recently even nanosheets, have been intensively investigated for their peculiar opto-electronic properties related to the quantum confinement effect.[1,2,3,4,5,6,7,8,9] Among them, cadmium based II-VI colloidal nanocrystals have received most of the attention, due to the well-established synthesis routes, a photoluminescence (PL) peak that is tunable over the entire visible spectrum, and a high photoluminescence quantum efficiency, exceeding 50% in core/shell systems.[10,11] Next to the linear optical properties, quantum confinement also allows to control the nonlinear absorption coefficient. More specifically, Qrods can exhibit a large two-photon absorption (2PA) cross section,[12,13] and the concomitant efficient sub-band gap excitation of the photoluminescence is of great interest for applications in photonic and optoelectronic devices. Consequently, several studies have proposed them as suitable candidates for two-photon pumped bio-labels,[14] or as active materials in lasing[15,16,17] and optical data storage.[18,19]

Experimental and theoretical studies that focused on an improved fundamental understanding of 2PA in colloidal nanocrystals have revealed that in the limit of strong confinement, for instance experienced by small PbS and PbSe nanocrystals, quantum confinement may also weaken the optical selection rules, giving rise to one-photon allowed transitions in 2PA spectra and *vice versa*.[20,21] Surprisingly, two-photon induced photoluminescence excitation (2PPLE) spectra for cadmium chalcogenides have been less investigated. Blanton *et al.*[22] already showed more than

15 years ago that for spherical CdSe Qdots, data are in fact well reproduced by *k.p* calculations, which was confirmed on CdTe Qdots in more recent years.[23,24] Additionally, despite well established synthesis routes for various cadmium-based core/shell nanocrystals, only few reports exist on multiphoton absorption in heterostructured nanocrystals.[13,25,26] It is however well known that moving from a single-composition CdSe Qdot to a heterostructured system can present several advantages. In our case for instance, CdSe/CdS quasi-type II heterorods (Qrods) are efficient emitters, with an emission wavelength that can be controlled almost independently from the growth of the CdS shell, which constitutes the major contribution to the absorption process. Moreover, the large shell volume can reduce the luminescence re-absorption, a common issue in optically thick samples, and the rod shape itself is known to provide linearly polarized absorption and emission.[27,28]

In this work we have explored the 2PA properties of core/shell Qrods, and compared them to spherical CdSe core-only Qdots. From a practical perspective, the Qrod PL is more resistant to photobleaching than CdSe Qdots, and the growth of a long CdS Qrod shell over the CdSe core conveniently allows decoupling the PL emission spectrum from the enhanced 2PA at higher energies. More importantly however, the spectral dependence of the 2PPLE yields a significant blue shift for optical transitions in both the CdSe core and CdS shell spectral region. Experimental data are confirmed by *k.p* calculations, taking into account both the effect of band anisotropy (anisotropic hole masses), and the reduced symmetry of the confining potential, due to the rod shape of the CdS shell.

Results and discussion

Two-photon absorption cross section. In figure 1a, we compare the luminescence spectrum of typical CdSe/CdS Qrods, excited under one- and two-photon conditions, respectively. There are no remarkable differences in the luminescence induced by the two different types of

excitation. The 2PA-induced spectrum shows a red shift of the intensity maximum of 1.7+/- 0.1 nm, which can be explained by a slight difference in temperature of the sample, probably induced by the more intense irradiation during the nonlinear PL measurements. More importantly, a single-exponential PL decay is observed under both types of excitations (figure 1b, sample HB2), with no remarkable difference in decay time. We obtained 12.1 +/- 0.2 ns and 12.0 +/- 0.1 ns for the one-photon and two-photon decay times, respectively (figure 1b), with 2PA-induced decay times in the range 8-15 ns found for the other core/shell Qrods. These are all comparable with the typical decay times reported for CdSe/CdS Qrods,[17,29] hence our findings are in agreement with the hypothesis that the 2PA creates a single electron-hole pair that relaxes *via* non-radiative intraband transitions to the band-edge, where it recombines predominantly radiatively.

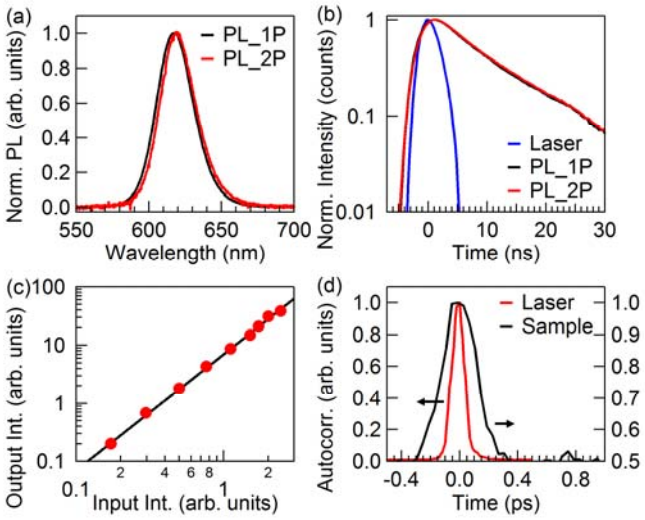

Figure 1: (a) Normalized fluorescence spectra of a typical CdSe/CdS Qrod sample, excited under one-photon (black curve, at 400 nm) and two-photon conditions (red curve, at 800 nm). The slight difference in the peak position can be ascribed to a small temperature increase of the sample under 2PA pumping. (b) Normalized fluorescence decay traces of CdSe/CdS Qrods (sample HB2), excited with nanosecond pulses. The one-photon induced decay (red curve, excitation at 425 nm) compares well with the two-photon induced decay (green curve, exciation at 850 nm). The black curve gives the time response of the detector (equal to 1.8ns). (c) Typical dependence of the 2PPLE on the input power (sample HB2). The line is a quadratic fit to the data points. (d) Femtosecond autocorrelation measurements at 800nm for the laser pulses (red curve) and fluorescence of a CdSe/CdS Qrod sample (black curve). A gaussian fit yields a peak width of 276 fs (full-width at half maximum) for the latter, comparable to the laser pulse autocorrelation of 104 fs.

The amplitude of the PL signal was well fitted with a quadratic dependence on the input power (figure 1c). Such behavior was observed for all Qdot and Qrod samples, under both nanosecond and femtosecond excitation, with a power-law fit giving a value varying between 1.8 and 2.1. In order to further confirm that the 2PA of the sample is due to a pure nonlinear process rather than mediated by linear absorption *via* intermediate long-living trap states, an autocorrelation experiment was performed under femtosecond pulsed excitation (figure 1d). In the experiment, two portions of the 800nm laser beam are superposed in the sample cell, but their relative delay is varied. Since long-lived trap states in CdSe nanocrystals have a decay time of more than 100 ns (see supporting information, figure S1), i.e. far longer than the 100 fs pulse duration, the autocorrelation peak width supports a purely nonlinear effect not mediated by real states. The slightly larger FWHM for the measurement in the sample can be explained by a dispersion-induced temporal broadening of the pulse crossing the 1 mm sample thickness and by an increase of the region in which the two pulses are superposed inside the cuvette. Importantly, the results also allow us to safely extend the pulse duration to the ns-domain (as done for the measurement of the 2PA spectrum and cross section), as for 2PA, the pulse duration of the excitation laser merely influences the absolute amplitude of the two-photon induced PL and does change the 2PA cross section.

At 800 nm, the 2PA cross section of our CdSe/CdS Qrods lies in the range of 10^5 GM (figure 2a, see table S1 in supporting information for structural parameters of the Qrods). From a single-Qdot point of view, the results found here are consistent with those of Li *et al.*[12] and Xing *et al.*[13]; they reported a value of 2 10^5 GM (CdS Qrods) and 0.3-14 10^5 GM (CdSe/CdS Qrods), respectively. We observe an enhancement of about two orders of magnitude for the 2PA cross section compared to a spherical CdSe Qdot sample, where we find a value of 2.10^3 GM. Except for CdTe Qdots,[30] data on spherical CdS,[12] CdSe,[30] and CdSe/CdS Qrods,[13] including the ones

presented here, all show a linear dependence of the cross section on the nanocrystal volume (figure 2a). The strong enhancement of 2PA cross sections for CdS and CdSe/CdS Qrods is therefore mainly due to the increased volume. Indeed, once normalized over the volume, results for the different CdSe/CdS Qrods measured lead to an average value of 150±50 GM/nm^3, and data agree well with previous results obtained at 800 nm on CdS,[12] CdSe[30] and CdSe/CdS heteronanocrystals.[13] They observed an average 2PA cross section of 100±7 GM/nm^3, 150±25 GM/nm^3, and 180±30 GM/nm^3, respectively.

A comparison of the data for CdS Qdots and CdS and CdSe/CdS Qrods suggests that the volume-normalized 2PA cross section is slightly larger for anisotropic Qrods than for spherical Qdots, which might be due to a reduced average screening of the electric field in rod-shaped nanocrystals. More importantly however, it should be stressed that the CdSe/CdS heteronanocrystals present the advantage of decoupling the emission wavelength from the nonlinear absorption provided by the CdS shell. Hence we can enhance the 2PA cross section for any predefined wavelength, while in single-composition Qdot and Qrods a large 2PA cross section can only be obtained in nanocrystals of higher volume, with concomitantly reduced quantum confinement and redshifted emission. Furthermore, due to the growth of a CdS shell, the CdSe/CdS Qrods are much more resistant to photobleaching when exposed to continuous illumination, as their 2PA induced PL typically does not vary by more than 10%, even after 90 minutes of excitation (figure 2(b)). CdSe core Qdots on the other hand lost in some cases up to 70% of their initial PL after the same amount of time.

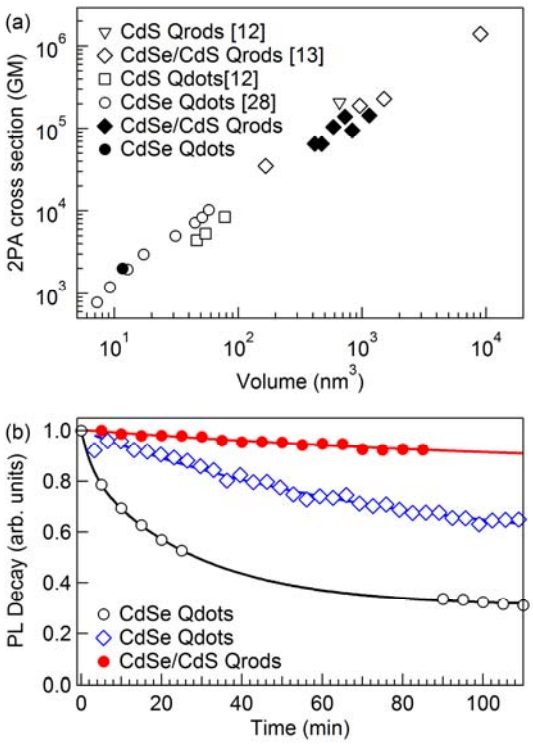

Figure 2: (a) 2PA cross section per particle for different samples (open symbols: literature results, full symbols: present data). The 2PA cross section increases linearly with particle volume in all cases. (b) Decay of two-photon induced PL. Two typical examples of CdSe Qdots (open symbols) are compared to CdSe/CdS Qrods (full symbols), which only show a 10% drop in PL after 90 minutes of continuous illumination. Lines added as guide to the eye.

Two-photon induced excitation spectrum. The large 2PA cross section at 800nm combined with the control over the emission wavelength already highlights the advantage of using heterostructured nanocrystals. Nevertheless, as we excite close to the CdS band edge, only the spectral dependence of the 2PA can reveal which wavelengths are most suitable for two-photon excitation. Moreover, the spectrum can yield a better understanding of the underlying opto-electronic band structure.[22,23,24,31] Figure 3 shows a typical 2PA spectrum (all measurements performed in tetrachloro ethylene, TCE, using ns-pulses) obtained on a sample of core/shell Qrods (b), compared to a spectrum for a typical CdSe Qdot suspension (a). In both cases, the one-photon absorption spectrum is shown in the same graph as well. The 2PA spectra obtained

on CdSe Qdots with diameter varying from 2.5 nm to 4 nm (see supporting information, figure S3), are comparable with previous literature reports. They show a first 2PA peak at an energy that is higher with respect to the energy for the first one-photon absorption peak. The blue shift of 85 nm agrees perfectly with values reported in similar measurements at 5K.[22,32] Remarkably, similar results are obtained on the Qrod samples: the nonlinear absorption of the core is strongly blue shifted compared to the linear spectrum, and also in the region of the CdS shell transitions, the onset of 2PA starts at an energy that is noticeably higher than the corresponding absorption edge observed under 1PA excitation.

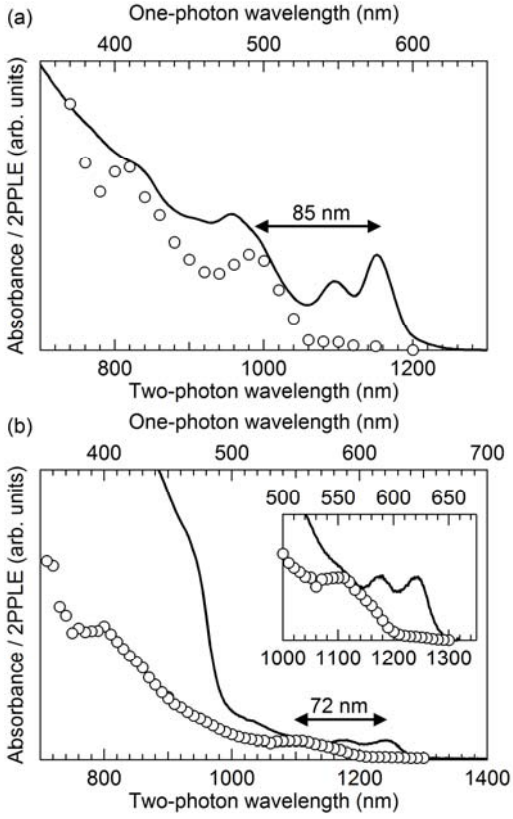

Figure 3: (a) Comparison of the absorbance (full line) and 2PPLE (symbols) spectra for a sample of 2.9 nm CdSe Qdots. A blue shift of 85 nm is observed for the first transition (b) Absorbance (full line) and 2PPLE (symbols) spectrum for CdSe/CdS Qrods HB5. A blue shift of 72 nm is measured. Inset: detail of the band-edge absorption. All samples, consisting of different core diameters, and rod diameters and lengths, showed similar results (see supporting information, figure S4).

It is well known that the differences in the one- and two-photon absorption spectra arise from the different selection rules that these transitions have to obey. In the dipole approximation, only transitions coupling electron and hole states characterized by the same angular momentum are allowed *via* one-photon absorption (1PA) while different selection rules apply for 2PA, which leads to different absorption peaks in the spectra.[22,32] For spherical Qdots, the first peak is generally blue-shifted in the case of 2PA. In fact, additional transitions observed for PbSe and PbS Qdots, resonant with dipole-allowed 1PA peaks, triggered a long-standing debate in literature whether they were due to a reduced symmetry of the confining potential in these crystals or if results could be explained by band structure anisotropy, with a substantial amount of experimental evidence and theoretical calculations supporting both hypotheses.[20,33,34,35] The data suggest that, although band anisotropy cannot be neglected as it gives rise to additional transitions due to a splitting of the electron and hole P-states, only the inclusion of symmetry breaking leads to an enhancement of 2PA at the spectral position where the first one-photon transition is observed.[21]

***k.p* calculations.** To obtain a better understanding of the selection rules that govern the blue shift of the 2PA spectrum in anisotropic CdSe/CdS Qrods, and the nature of the transitions at wavelengths below the CdS 1PA onset, we used 1-band *k.p* calculations. We modeled three different structures and compared their theoretical 1PA and 2PA with the experimental values: (i) a core-only Qdot with diameter 4.4 nm; (ii) a heterorod with a small core (sample HB1, see table 1) and (iii) a heterorod with a large core (sample HB5). The corresponding low-lying energy levels are plotted in figure 4a, 4b and 4c, respectively.

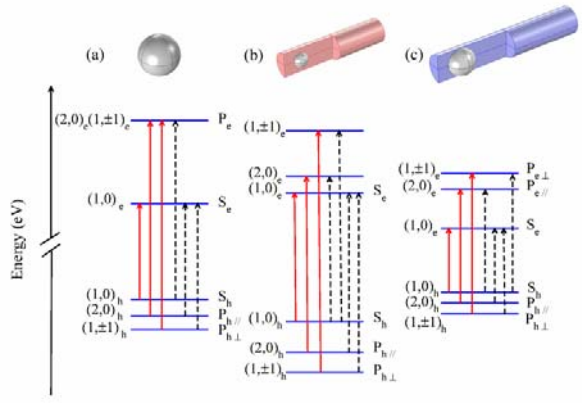

Figure 4: Near-gap energy levels and 1PA (red, solid arrows) and 2PA (black, dashed arrows) dipole-allowed transitions for (a) a core-only quantum dot with diameter 4.4 nm, (b) a heterorod with a small core (sample HB1 in table I), and (c) a heterorod with a large core (sample HB5). The states localized near the core are labeled with both axial and spherical symmetry notations.

Because all three structures have axial symmetry, the electron and hole states can be labeled as $(n,m)_j$, where $n=1,2,3\ldots$ is the main quantum number, $m=0,\pm1,\pm2\ldots$ the envelope angular momentum projection and $j=e,h$ stands for electron or hole. For states confined in the core, we also give the conventional notation of spherically symmetric states, nL_j, where L=S,P,D… represents the envelope angular momentum. Owing to the anisotropic hole masses, the P_h shell is split into $P_{h||}$ and $P_{h\perp}$. Instead, the conduction band is nearly isotropic, so the P_e shell does not split. This is in contrast with PbSe and PbS Qdots, where both conduction and valence band are anisotropic.[21] We note that strictly speaking there are no states truly confined to the core or the shell, as there is always some part of the wavefunction leaking into the entire heterostructure. However, we find that some electron and hole states are *mainly* confined to the spherical core, even at energies exceeding the respective band offsets. In figure 4, we label these states using both axial and spherical notation. One can see that the Qrod HB1 –where the core is only 2.5 nm– behaves as a quasi-type-II heterostructure, with only the ground state of electrons ($1S_e$) and a few of the lowest-lying states of holes ($1S_h$ and $1P_h$) confined to the core and the other

states delocalized over the rod. By contrast, in HB5 the core is 5 nm, and it can host also $1P_e$ and higher excited electron and hole states.

The vertical arrows in figure 4 show the dipole-allowed 1PA (red, solid lines) and 2PA (black, dashed lines) transitions. For spherical quantum dots the selection rules are usually understood in terms of conservation of the even/odd parity with respect to the inversion symmetry.[21] When the symmetry is lowered to $C_{\infty v}$, as in our Qrod heterostructures, the only selection rule remaining is related to the conservation of the azimuthal angular momentum *m*. For 1PA processes the selection rule is given by $\Delta m=m_e-m_h=0$ and for 2PA processes it is given by $\Delta m=0,\pm1$.

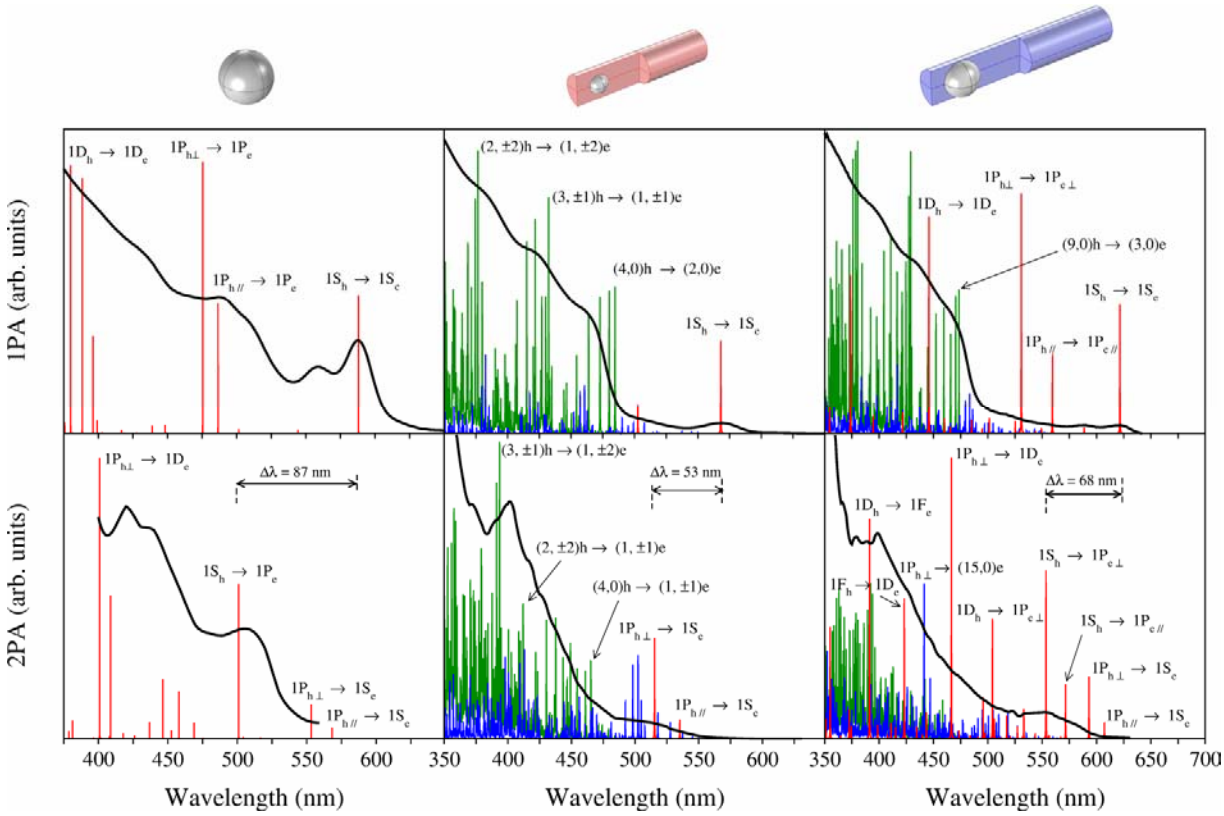

Figure 5: 1PA (top) and 2PA (bottom) experimental and calculated spectra for the CdSe Qdots (left), CdSe/CdS Qrods HB1 (middle) and CdSe/CdS Qrods HB5 (right). To facilitate the comparison between linear and non-linear resonances, the wavelength in the horizontal axis has been set equal to the photon wavelength for the 1PA spectra and to half the photon wavelength for the 2PA spectra. The calculated absorptions are colored according to the location of the initial and final states involved in the transition: dot-dot (red), dot-rod (blue), and rod-rod (green). Black lines represent the experimental data

When analyzing the absorption spectra, one finds that many allowed transitions turn out to have very weak intensity. This can be understood by considering that the potential felt by low-energy states confined in the core is essentially that of a sphere with inversion symmetry. Parity is then an approximate quantum number. The same occurs with high-energy states of the rod which barely feel the core potential. This adds new restrictions to the selection rules above. Namely, for 1PA (2PA) transitions the parity of the initial and final states must be the same (different). Figure 5 shows the calculated 1PA and 2PA for the three structures under study compared to the experimental measurements. Some of the main transitions are labeled by the quantum numbers of the initial (hole) and final (electron) state, using spherical notation for states localized in the core.

We start by analyzing the absorption spectrum of the spherical Qdots (left panels). The 1PA spectrum shows that the low energy experimental resonances can be explained fairly well by the $1S_h \rightarrow 1S_e$, $1P_h \rightarrow 1P_e$ and $1D_h \rightarrow 1D_e$ transitions. Only the second absorption peak (near λ~560 nm) misses a clear assignment. Previous studies have predicted the $2S_h \rightarrow 1S_e$ transition next to the fundamental one.[22,36] This transition is suppressed in our model by the spherical symmetry and strong confinement, which lead to nearly orthogonal $2S_h$ and $1S_e$ states. However, recent experimental data suggest that this transition is influenced by both the Qdot crystal structure and organic ligands,[37] hence surface functionalization and related atomic rearrangements of the nanocrystal surface, which are not captured by our theoretical model, may change the $2S_h \rightarrow 1S_e$ oscillator strength. In the 2PA spectrum, the low-energy peaks can be well described by the transitions between 1P and 1S states of electrons and holes. The most important result here is that the experimental blue shift between the first intense 1PA and 2PA peaks is in good agreement with the theoretical shift between $1S_h \rightarrow 1S_e$ and $1S_h \rightarrow 1P_e$ transitions ($\Delta\lambda$~87 nm, see figure). Interestingly, there are dipole-allowed 2PA transitions at lower energy (namely $1P_{h\perp} \rightarrow 1S_e$ and $1P_{h\parallel} \rightarrow 1S_e$) which would translate into smaller blue

shifts. However, these turn out to be much weaker than the $1S_h \rightarrow 1P_e$ transition. This can be understood from the denominator in the perturbational estimate of the transition rate, W_{2PA} (see equation (2) of Methods). The strongest 2PA transitions are those where the intermediate state energy is close to that of the resonant photon, $E_i \approx (E_v + E_c)/2$. As illustrated in figure 6(a), the $1S_h \rightarrow 1P_e$ transition takes place mainly through the intermediate states $1S_e$ and $1P_h$, while the $1P_h \rightarrow 1S_e$ transitions (figure 6b) takes place mainly through $1S_h$ and $1P_e$. Because electron states have a larger energy splitting, one can easily see that the intermediate state $1S_e$ is closest to the resonance condition (dashed line).

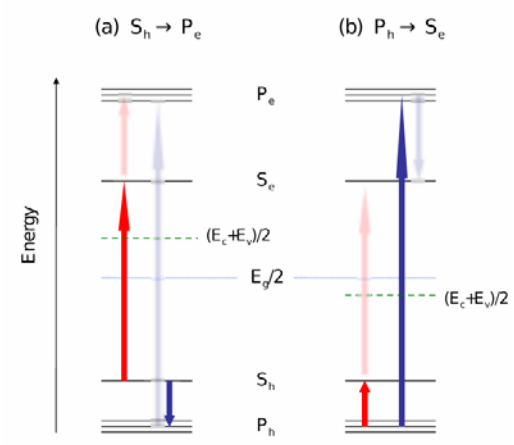

Figure 6: Most important excitation paths contributing to the 2PA transition rate of (a) $1S_h \rightarrow 1P_e$ and (b) $1P_h \rightarrow 1S_e$ absorptions. Red and blue arrows are used for different paths. The bright arrow shows the transition to the intermediate state in each case.

Next, we analyze the absorption of heterorods. Central panels in figure 5 show the spectra of sample HB1. The 1PA peaks are well reproduced by the theoretical transitions. Because the core of this structure is 2.5 nm, only the lowest energy transition involves states localized in the core ($1S_h \rightarrow 1S_e$). Most of the higher energy peaks arise from states essentially localized in the rod. Since the longitudinal confinement of the rod is weak, there are bunched groups of states with similar energy, which share the same angular momentum *m* but have different *n* (i.e. number of nodes in the growth direction). This gives rise to branches of transitions for each *m*,

e.g. those dominated by $(4,0)_h \rightarrow (2,0)_e$, starting at λ≈490 nm, or those dominated by $(3,1)_h \rightarrow (1,1)_e$, starting at λ≈430 nm. The 2PA spectrum of HB1 is more complicated than that of the simple Qdot because the CdS shell provides a high density of intermediate states. The fundamental transition is now $1P_{h\perp} \rightarrow 1S_e$, because the $1P_e$ state is no longer localized in the core. The blue shift of this transition with respect to the fundamental 1PA one is ~53 nm, slightly reduced compared to the shift observed in core-only CdSe Qdots, and again close to the experimental value. A significant shift is also observed in the CdS shell absorption region between the sharp onset of the high-energy 1PA absorption and the most intense 2PA transitions, consistent with the experimental data. In this region, the intensity of 1PA transitions increases swiftly whenever the resonant photon reaches a new *m* shell, which translates into a steep increase of the 1PA spectrum. Conversely, the increase of the 2PA intensities is more gradual, explaining the gentler slope of this spectrum.

The fact that the $(3,1)_h \rightarrow (1,2)_e$ transition dominates the 2PA –giving rise to the shell blue shift with respect to the 1PA spectrum– may be surprising because there are other symmetry-allowed two-photon transitions at lower energy. Yet, the oscillator strength of these transitions is much weaker. The reason is similar to that argued in figure 6 for the CdSe Qdot transitions. Namely, transitions between states near the band edge necessarily imply intermediate states with large values of $E_i - (E_v + E_c)/2$. These imply large denominators in W_{2PA}, and are generally inefficient. However, if the initial or final states are excited, intermediate states close to $(E_v + E_c)/2$ become available and W_{2PA} is greatly enhanced.

Right panels in figure 5 show the absorption spectra of the system HB5. Even though there are a few discrepancies when comparing to the experimental measurements (for example, for 1PA the strong $1P_{h\perp} \rightarrow 1P_{e\perp}$ transition is not observed at the predicted energy), the general features are again consistent. In particular, due to the reduced confinement in HB5 (core diameter 5.0 nm) compared to HB1 (core diameter of 2.5 nm), the $1P_{h\perp} \rightarrow 1S_e$ and $1P_{h\parallel} \rightarrow 1S_e$ 2PA

transitions are clearly closer to the fundamental $1S_e \rightarrow 1S_h$ 1PA transition (31 nm blue shift). However, the larger CdSe core diameter also gives rises to electron P-states confined to the core, yielding additional strong $1S_h \rightarrow 1P_e$ 2PA transitions in the CdSe band-edge spectral region. Moreover, in HB5 the core diameter is similar to that of the rod. Unlike for HB1, the energy scales of the core and rod states are comparable, leading to mutual interactions and a spectrum which is not just the direct sum of the two parts of the heterostructure. As a result, the $1P_e$ state splits into $1P_{e\perp}$ and $1P_{e||}$, not because of the mass anisotropy (as was the case for holes) but because of the asymmetric shell. Consequently, the fundamental 2PA transition is not simply $1S_h \rightarrow 1P_e$, as expected for core-only structures (left panels). Instead, we calculate a low energy $1S_h \rightarrow 1P_{e||}$ transition and a high energy $1S_h \rightarrow 1P_{e\perp}$ transition at λ~575 nm and λ~555 nm, respectively. As the oscillator strength of the $1S_h \rightarrow 1P_{e||}$ transition is 3 times weaker than the $1S_h \rightarrow 1P_{e\perp}$, the resulting 68 nm blue shift between the fundamental $1S_h \rightarrow 1S_e$ 1PA transition and the $1S_h \rightarrow 1P_e$ 2PA manifold is again in good agreement with experimental data. Clearly, compared to single composition Qdots, quasi-type II heterostructures, with a varying number of states localized near the core region depending on the extent of quantum confinement, provide an interesting additional mechanism to control the 2PA absorption spectrum (*in casu* the large blue shift between the fundamental 1PA and 2PA transitions).

Also in the spectral region of the shell absorption, the similar core and shell diameter gives rise to synergistic effects. Here, the spectrum comprises not only rod-to-rod transitions (colored green in figure 5) but now also dot-to-rod (blue) and even dot-to-dot (red) ones. In fact, transitions between high-energy states of the core have a non-negligible contribution to the high-energy absorption. Altogether, dot-to-rod and dot-to-dot absorptions amount up to 21% of the total 1PA in the CdS shell absorption region (resonant energies above the CdS band gap). This percentage increases up to 42% in the case of 2PA, of which 22% corresponds to high-energy dot-to-dot transitions. Figure 7 illustrates the states involved in the three types of high-

energy absorptions. The most intense rod-to-rod transitions take place between states localized mainly in the shell (figure 7a). These exhibit negligible tails in the core which gather most nodes to warrant orthogonality with the lower-lying core state(s) with the same azimuthal symmetry. By contrast, the relevant dot-to-rod transitions (figure 7b) may involve a delocalized state that spreads uniformly throughout the entire heterostructure. These transitions gain significance in the non-linear spectrum owing to the participation of intermediate states, thus overcoming the small overlap between the initial and final states that limits their contribution to the linear absorption. But perhaps the most striking finding is the presence of intense dot-to-dot transitions at energies exceeding the CdS band gap. The reason is that one (typically the electron) or even both states involved in the transition can lie above the corresponding band offset and yet remain mainly localized in the core region. This counterintuitive result can be understood by considering that, owing to (i) the similar diameter of the core and the shell, and (ii) the large anisotropy of the confining potential, the lowest-lying states of each symmetry *m* can be described in the adiabatic approximation. Thus, the weak longitudinal confinement can be reasonably assumed to be decoupled from the strong in-plane one. The electron (or hole) in a given in-plane state of motion moves then in an effective 1D heterorod potential, but that is offset from the corresponding band edge by an amount given by the energy of the in-plane motion. As a consequence, at least the ground state of each symmetry *m* turns out to be mainly localized in the core region regardless of the associated in-plane energy, which can easily overcome the band offset.

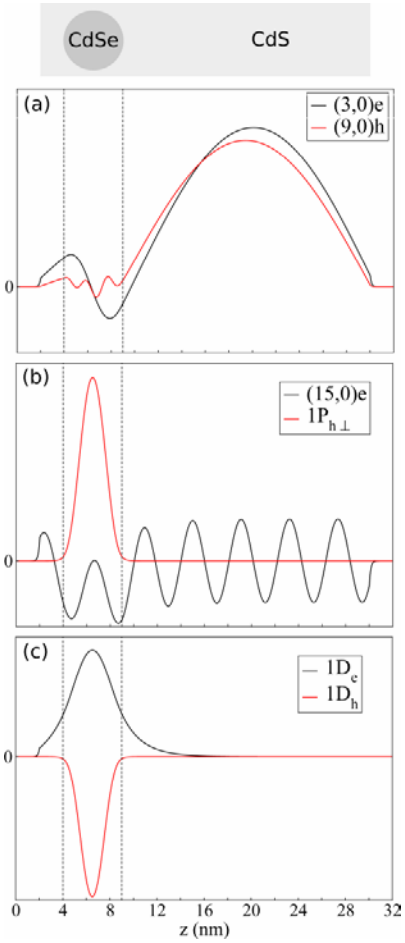

Figure 7: Typical examples of the longitudinal profiles of the initial and final states involved in the three types of absorptions arisen in CdSe/CdS Qrod HB5 beyond the CdS gap: (a) rod-to-rod, (b) dot-to-rod, and (c) dot-to-dot transitions. Vertical dashed lines indicate the Qdot spatial limits. The Qdot and Qrod nomenclature refers only to the region where the corresponding states of the system are mainly localized.

Figure 7c shows the states involved in a typical dot-to-dot transition showing up above the CdS band gap. It is worth noticing that the electron wave function shows an asymmetric leakage into the rod region, a feature also shared by the ground and lowest-lying electron states below the band offset. Despite such asymmetry, neither the experimental nor the simulated data reveal signatures of parity symmetry breaking in these states.[38] The reason is connected with the strong localization of the hole in the dot. Only the region where the electron and hole wavefunctions overlap contributes to the transition rates (see matrix elements in Eqs.1 and 2),

and inside the Qdot core the electron wavefunction is almost symmetric (see figure 7c). Hence, despite the explicit presence of an anisotropic electron wavefunction induced by the electron delocalization in the shell, our experimental and theoretical data on the different CdSe/CdS core/shell Qrods do not reveal any spectral evidence for symmetry breaking. Experiments thus suggest that it has a material-dependent origin, being stronger in PbS and PbSe Qdots, compared to cadmium-based materials such as the CdSe Qdots and CdSe/CdS Qrods. Since in CdSe the exciton Bohr radius is around 5.5 nm, while for PbS and PbSe it is 4 and 8 times higher, respectively, results suggest that the lower extent of quantum confinement in CdSe/CdS Qrods lies at the origin of the differences observed.

Conclusions

We have measured 2PPLE spectra on CdSe Qdots and CdSe/CdS core/shell Qrods, having different lengths, and rod and core diameters. We observed that 2PA in nanocrystals is an intrinsically nonlinear phenomenon, i.e. it does not involve transitions through long-living inter-band trap states. The absolute values of the cross section are in the range of 10^5 GM in the heterostructured Qrods samples, consistent with results on similar Qrod samples in literature,[12,13] and with the clear advantage of independent control over the emission wavelength and the 2PA absorption cross section. It suggests a large potential for such structures in multi-photon excitation applications like bio-imaging or as nonlinear gain media. 2PA spectra from our CdSe/CdS heterorod samples show transitions that are blue shifted in energy, i.e. we did not find evidence of selection rule violations, despite the explicit inclusion of a reduced symmetry of the confining potential *via* the anisotropic shape of the quasi-type II Qrod. This reinforces the hypothesis that the breaking of the optical selection rules is only observed under conditions of

exceptionally strong quantum confinement, as is the case in lead chalcogenide Qdots, rather than merely an asymmetrical shape of the crystal.

The numerical simulations of the dipole allowed transitions based on effective mass models show a good agreement with the experimental data, and corroborate that the observed blue shifts are a consequence of (i) the different selection rules that apply to 1PA and 2PA transitions despite the valence band and confinement anisotropies, and (ii) the reduced oscillator strength of low-energy two-photon transitions. Furthermore, the blue shift can be controlled by the degree of quantum confinement in quasi-type II Qrods, more specifically by localizing also the electron P-states near the CdSe core region, which gives rise to a strong $1S_h \rightarrow 1P_e$ transition.

The calculations finally reveal a rich interplay between the core and shell transitions of the heterorods. This becomes apparent in the high-energy absorption, which comprises not only rod-to-rod but also dot-to-rod and even dot-to-dot transitions with a non-negligible contribution. The latter ones involve electron and hole states which are mainly localized in the spherical core despite exceeding energetically the band offset, a result that can only be understood by considering the heterorod as a unique system, more complex than the mere sum of its constituents.

Methods

CdSe core Qdots and CdSe/CdS core/shell Qrods were synthesized according to established literature methods. The Qrod diameter and length were determined by transmission electron microscopy (TEM), giving lengths ranging from 20 nm to 60 nm and diameters spanning 4 nm to 7 nm (average values, obtained by measuring the dimensions of at least 100 particles). Properties of the Qrod samples used for the 2PPLE measurements are summarized in table 1. After synthesis, they were dispersed in toluene or TCE, depending on the 2PA wavelengths

examined (toluene shows distinct absorption peaks beyond 1100 nm, requiring the use of optically transparent TCE). Typical Qdot/Qrod concentrations in the optical experiments varied between 5 and 20 nM for the rods and between 20 and 200 nM for the dots. The concentration was determined using the absorption of the Qdot/Qrod solution at 295 nm, according to methods described in ref [39]. Briefly, it is calculated taking into account the different local field factors associated with their respective size and shape, and using the optical constants of bulk CdSe[40] and CdS.[41]

sample	Core diameter	Rod diameter	Rod length
	nm	nm	nm
HB1	2.5	4.5	20
HB2	3.8	5.8	35
HB3	3.8	5.8	23
HB4	3.4	4.2	22
HB5	5.0	5.2	28

Table 1: Structural parameters of the CdSe/CdS Qrods used for the 2PPLE spectra, as determined by TEM.

For the 2PPLE spectroscopy, we used a laser beam coming from an optical parametric oscillator operating in the nanosecond regime (Vibrant IIE, OPOTEK, 410-2000 nm wavelength range, 10 Hz repetition rate, maximum energy per pulse of 6 mJ). The beam was focused to a diameter of approximately 1 mm in the center of a 10 mm thick quartz cell. Two-photoninduced PL from the sample was collected at a 90° angle with respect to the excitation. Alternatively, an amplified Ti:Sapphire laser (Coherent, 800 nm wavelength, 1 kHz repetition rate, maximum energy per

pulse of 30 uJ), was used in the same geometry. Again, the excitation beam was focused in the optical cell, here to a spot size of approximately 0.5 mm.

The PL was collected by a photomultiplier tube (PMT) coupled to an oscilloscope. The PMT was continuously calibrated against a reference photodiode that collected part of the incoming beam using a 5% beamsplitter. The photodiode response itself was quantified with a power meter for the femtosecond laser and with an energy meter for the nanosecond laser, placed just in front of the sample position. In each measurement series, to ensure that samples were unaffected by the strong excitation intensity, we verified that luminescence spectra and decay lifetimes of the Qrods, obtained *via* 2PA at 800 nm, were comparable to the luminescence spectra obtained by one-photon induced PL employing a 400 nm light source.

At all wavelengths, we verified the quadratic dependence of the 2PA by measuring the PL signal as function of input power. To determine the absolute 2PA cross section of the Qrods, the 2PA cross section of Rhodamine B in methanol was used as a reference.[42] Luminescence signals were normalized over the respective concentrations of the samples and over the emission quantum efficiency of samples and reference dye.

Numerical simulations of 1PA and 2PA transition rates were obtained from first and second-order Fermi golden rules:

$$W_{1PA} = \frac{2\pi}{\hbar}\sum_{c,v}|\langle c|\boldsymbol{e}\cdot\boldsymbol{p}|v\rangle|^2\,\delta(E_c - E_v), \qquad (1)$$

and

$$W_{2PA} = \frac{2\pi}{\hbar}\sum_{c,v}\left|\sum_{i}\frac{\langle c|\boldsymbol{e}\cdot\boldsymbol{p}|i\rangle\langle i|\boldsymbol{e}\cdot\boldsymbol{p}|v\rangle}{E_i - E_v - \hbar\nu}\right|^2\delta(E_c - E_v - 2\hbar\nu). \qquad (2)$$

where *hv* is the photon energy, *e* is the polarization vector of the light, *c* and *v* are the final (conduction band) and initial (valence band) states, and *i* labels the intermediate states of the two-photon transition, which are the one-photon accessible states in the valence or conduction bands.

Electron and hole states in equations (1) and (2) were calculated within the *k·p* formalism in the single-band, single-particle approximation. This simple model captures the effect of the confinement strength and symmetry, which suffices to explain the experimentally observed blue shifts,[43] as we shall see below. In cylindrical coordinates and atomic units, the corresponding three-dimensional effective mass Hamiltonians read[44]

$$H_j = -\frac{1}{2\rho}\frac{\partial}{\partial\rho}\left(\frac{\rho}{m^*_{j,\rho}(\rho,z)}\frac{\partial}{\partial\rho}\right) - \frac{1}{2}\frac{\partial}{\partial z}\frac{1}{m^*_{j\|}(\rho,z)}\frac{\partial}{\partial z} + \frac{m_j^2}{\rho^2 m^*_{j\perp}(\rho,z)} + V_j(\rho,z) \quad (3)$$

In equation (3), *j=e,h* denotes the electron and hole, respectively, m_j is the azimuthal angular momentum, and $V_j(\rho,z)$ is the spatial confinement potential. At the CdSe/CdS interface, $V_j(\rho,z)$ presents a step-like profile determined by the corresponding band offset. $m^*_{j\perp}(\rho,z)$ and $m^*_{j\|}(\rho,z)$ are the position-dependent transversal and longitudinal effective masses, respectively. The valence band anisotropy of both CdSe and CdS leads to anisotropic hole masses, which are heavier along the longitudinal (growth) direction. We used $m^*_{h\|}=1.19m_0$ and $m^*_{h\perp}=0.48m_0$.[45] In contrast, the electron effective mass can be considered isotropic in the conduction band, though different for core ($m^*_{e,CdSe}=0.13m_0$) and shell ($m^*_{e,CdS}=0.17m_0$) materials.[45,46] The CdSe core was modeled as a sphere embedded in a cylindrical CdS shell, 2 nm away from its base (see insets in figure 4). The valence band offset at the heterojunction is 0.44 eV and the conduction band one is 0.3 eV.[6,45,46] The whole structure is surrounded by a 4 eV potential barrier. By means of a finite differences scheme, the Hamiltonians in (3) were integrated numerically to obtain electron

and hole energies and wave functions. Finally, the energy gap was taken so as to fit the fundamental $1S_h \rightarrow 1S_e$ transition with the energy of the first experimental 1PA peak.

Supporting information

Structural parameters of the CdSe/CdS Qrods used for the measurement of the 2PA cross section, CdSe photoluminescence lifetime of the trap emission and estimated effect of long-lived trap states on the fluorescence autocorrelation, additional 2PPLE spectra for CdSe core Qdots and CdSe/CdS core/shell Qrods, plots of the relevant electron and hole wavefunctions, and assessment of the effect of Coulomb interactions and a reduced conduction band offset in the *k.p* calculations. This material is available free of charge *via* the Internet at http://pubs.acs.org.

Acknowledgments

F. De Donato is acknowledged for providing CdSe and CdSe/CdS nanocrystal samples. The research leading to these results has received funding from the European Union's Seventh Framework Program (FP7/2007-2013) under REA grant agreement no. PIEF-GA-2011-298022 (NIRPLANA). Support from MICINN project CTQ-2011-27324, UJI-Bancaixa projects P1-1A2009-03 and P1-1B2011-01, and the Spanish FPI (MICINN) program (AB) is also acknowledged.

References

1. Efros, A. L.; Rosen, M.; Kuno, M.; Nirmal, M.; Norris, D. J.; Bawendi, M. Band-edge Exciton in Quantum Dots of Semiconductors with a Degenerate Valence Band: Dark and Bright Exciton States. *Phys. Rev. B* **1996**, *54*, 4843–4856.
2. Efros, A. L.; Rosen, M. The Electronic Structure of Semiconductor Nanocrystals. *Annu. Rev. Mater. Sci.* **2000**, *30*, 475–521.
3. Allan, G.; Delerue, C. Confinement Effects in PbSe Quantum Wells and Nanocrystals. *Phys. Rev. B* **2004**, *70*, 245321.
4. An, J. M.; Franceschetti, A.; Dudiy, S. V.; Zunger, A. The Peculiar Electronic Structure of PbSe Quantum Dots. *Nano Lett.* **2006**, *6*, 2728–2735.

5. Tischler, J. G.; Kennedy, T. A.; Glaser, E. R.; Efros, A. L.; Foos, E. E.; Boercker, J. E.; Zega, T. J.; Stroud, R. M.; Erwin, S. C. Band-edge Excitons in PbSe Nanocrystals and Nanorods. *Phys. Rev. B* **2010**, *82*, 245303.
6. Steiner, D.; Dorfs, D.; Banin, U.; Della Sala, F.; Manna, L.; Millo, O. Determination of Band Offsets in Heterostructured Colloidal Nanorods Using Scanning Tunneling Spectroscopy. *Nano Lett.* **2008**, *8*, 2954–2958.
7. Brovelli, S.; Schaller, R. D.; Crooker, S. A.; García-Santamaría, F.; Chen, Y.; Viswanatha, R.; Hollingsworth, J. A.; Htoon, H.; Klimov, V. I. Nano-engineered Electron–hole Exchange Interaction Controls Exciton Dynamics in Core–shell Semiconductor Nanocrystals. *Nat. Commun.* **2011**, *2*, 280.
8. Ithurria, S.; Tessier, M. D.; Mahler, B.; Lobo, R. P. S. M.; Dubertret, B.; Efros, A. L. Colloidal Nanoplatelets with Two-dimensional Electronic Structure. *Nature Mater.* **2011**, *10*, 936–941.
9. Rainò, G.; Stöferle, T.; Moreels, I.; Gomes, R.; Hens, Z.; Mahrt, R. F. Controlling the Exciton Fine Structure Splitting in CdSe/CdS Dot-in-Rod Nanojunctions. *ACS Nano* **2012**, *6*, 1979–1987.
10. Dang, C.; Lee, J.; Breen, C.; Steckel, J. S.; Coe-Sullivan, S.; Nurmikko, A. Red, Green and Blue Lasing Enabled by Single-exciton Gain in Colloidal Quantum Dot Films. *Nature Nanotech.* **2012**, *7*, 335–339.
11. Carbone, L.; Nobile, C.; Giorgi, M. De; Della Sala, F.; Morello, G.; Pompa, P.; Hytch, M.; Snoeck, E.; Fiore, A.; Franchini, I. R. *et al.* Synthesis and Micrometer-Scale Assembly of Colloidal CdSe/CdS Nanorods Prepared by a Seeded Growth Approach. *Nano Lett.* **2007**, *7*, 2942–2950.
12. Li, X.; Embden, J. van; Chon, J. W. M.; Gu, M. Enhanced Two-photon Absorption of CdS Nanocrystal Rods. *Appl. Phys. Lett.* **2009**, *94*, 103117.
13. Xing, G.; Chakrabortty, S.; Chou, K. L.; Mishra, N.; Huan, C. H. A.; Chan, Y.; Sum, T. C. Enhanced Tunability of the Multiphoton Absorption Cross-section in Seeded CdSe/CdS Nanorod Heterostructures. *Appl. Phys. Lett.* **2010**, *97*, 061112.
14. Larson, D. R.; Zipfel, W. R.; Williams, R. M.; Clark, S. W.; Bruchez, M. P.; Wise, F. W.; Webb, W. W. Water-Soluble Quantum Dots for Multiphoton Fluorescence Imaging in Vivo. *Science* **2003**, *300*, 1434–1436.
15. Jasieniak, J. J.; Fortunati, I.; Gardin, S.; Signorini, R.; Bozio, R.; Martucci, A.; Mulvaney, P. Highly Efficient Amplified Stimulated Emission from CdSe-CdS-ZnS Quantum Dot Doped Waveguides with Two-Photon Infrared Optical Pumping. *Adv. Mater.* **2008**, *20*, 69–73.
16. Todescato, F.; Fortunati, I.; Gardin, S.; Garbin, E.; Collini, E.; Bozio, R.; Jasieniak, J. J.; Della Giustina, G.; Brusatin, G.; Toffanin, S. *et al.* Distributed Feedback Laser: Soft-Lithographed Up-Converted Distributed Feedback Visible Lasers Based on CdS-CdZnS-ZnS Quantum Dots. *Adv. Funct. Mater.* **2012**, *22*, 337–344.
17. Xing, G.; Liao, Y.; Wu, X.; Chakrabortty, S.; Liu, X.; Yeow, E. K. L.; Chan, Y.; Sum, T. C. Ultralow-Threshold Two-Photon Pumped Amplified Spontaneous Emission and Lasing from Seeded CdSe/CdS Nanorod Heterostructures. *ACS Nano* **2012**, *6*, 10835–10844.
18. Li, X.; Bullen, C.; Chon, J. W. M.; Evans, R. A.; Gu, M. Two-photon-induced Three-dimensional Optical Data Storage in CdS Quantum-dot Doped Photopolymer. *Appl. Phys. Lett.* **2007**, *90*, 161116.
19. Dallari, W.; Scotto d'Abbusco, M.; Zanella, M.; Marras, S.; Manna, L.; Diaspro, A.; Allione, M. Light-Induced Inhibition of Photoluminescence Emission of Core/Shell Semiconductor Nanorods and Its Application for Optical Data Storage. *J. Phys. Chem. C* **2012**, *116*, 25576–25580.
20. Peterson, J. J.; Huang, L.; Delerue, C.; Allan, G.; Krauss, T. D. Uncovering Forbidden Optical Transitions in PbSe Nanocrystals. *Nano Lett.* **2007**, *7*, 3827–3831.

21. Nootz, G.; Padilha, L. A.; Olszak, P. D.; Webster, S.; Hagan, D. J.; Stryland, E. W. V.; Levina, L.; Sukhovatkin, V.; Brzozowski, L.; Sargent, E. H. Role of Symmetry Breaking on the Optical Transitions in Lead-Salt Quantum Dots. *Nano Lett.* **2010**, *10*, 3577–3582.
22. Blanton, S. A.; Hines, M. A.; Schmidt, M. E.; Guyot-Sionnest, P. Two-photon Spectroscopy and Microscopy of II--VI Semiconductor Nanocrystals. *J. Lumin.* **1996**, *70*, 253–268.
23. Padilha, L. A.; Fu, J.; Hagan, D.; Stryland, E. Van; Cesar, C.; Barbosa, L.; Cruz, C. Two-photon Absorption in CdTe Quantum Dots. *Opt. Express* **2005**, *13*, 6460–6467.
24. Qu, Y. L.; Ji, W. Two-photon Absorption of Quantum Dots in the Regime of Very Strong Confinement: Size and Wavelength Dependence. *J. Opt. Soc. Am. B* **2009**, *26*, 1897–1904.
25. Xing, G.; Ji, W.; Zheng, Y.; Ying, J. Y. Two- and Three-photon Absorption of Semiconductor Quantum Dots in the Vicinity of Half of Lowest Exciton Energy. *Appl. Phys. Lett.* **2008**, *93*, 241114.
26. Xing, G.; Chakrabortty, S.; Ngiam, S. W.; Chan, Y.; Sum, T. C. Three-Photon Absorption in Seeded CdSe/CdS Nanorod Heterostructures. *J. Phys. Chem. C* **2011**, *115*, 17711–17716.
27. Hu, J.; Li, L.; Yang, W.; Manna, L.; Wang, L.; Alivisatos, A. P. Linearly Polarized Emission from Colloidal Semiconductor Quantum Rods. *Science* **2001**, *292*, 2060–2063.
28. Kan, S.; Mokari, T.; Rothenberg, E.; Banin, U. Synthesis and Size-dependent Properties of Zinc-blende Semiconductor Quantum Rods. *Nature Mater.* **2003**, *2*, 155–158.
29. Rainò, G.; Stöferle, T.; Moreels, I.; Gomes, R.; Kamal, J. S.; Hens, Z.; Mahrt, R. F. Probing the Wave Function Delocalization in CdSe/CdS Dot-in-Rod Nanocrystals by Time- and Temperature-Resolved Spectroscopy. *ACS Nano* **2011**, *5*, 4031–4036.
30. Pu, S.-C.; Yang, M.-J.; Hsu, C.-C.; Lai, C.-W.; Hsieh, C.-C.; Lin, S. H.; Cheng, Y.-M.; Chou, P.-T. The Empirical Correlation Between Size and Two-Photon Absorption Cross Section of CdSe and CdTe Quantum Dots. *Small* **2006**, *2*, 1308–1313.
31. Padilha, L. A.; Nootz, G.; Olszak, P. D.; Webster, S.; Hagan, D. J.; Stryland, E. W. V.; Levina, L.; Sukhovatkin, V.; Brzozowski, L.; Sargent, E. H. Optimization of Band Structure and Quantum-Size-Effect Tuning for Two-Photon Absorption Enhancement in Quantum Dots. *Nano Lett.* **2011**, *11*, 1227–1231.
32. Schmidt, M. E.; Blanton, S. A.; Hines, M. A.; Guyot-Sionnest, P. Size-dependent Two-photon Excitation Spectroscopy of CdSe Nanocrystals. *Phys. Rev. B* **1996**, *53*, 12629–12632.
33. Franceschetti, A.; Luo, J. W.; An, J. M.; Zunger, A. Origin of One-photon and Two-photon Optical Transitions in PbSe Nanocrystals. *Phys. Rev. B* **2009**, *79*, 241311.
34. Goupalov, S. V. Selection Rules for Optical Transitions in PbSe Nanocrystal Quantum Dots: Drastic Effect of Structure Inversion Asymmetry. *Phys. Rev. B* **2009**, *79*, 233305.
35. Tudury, G. E.; Marquezini, M. V.; Ferreira, L. G.; Barbosa, L. C.; Cesar, C. L. Effect of Band Anisotropy on Electronic Structure of PbS, PbSe, and PbTe Quantum Dots. *Phys. Rev. B* **2000**, *62*, 7357–7364.
36. Norris, D. J.; Bawendi, M. G. Measurement and Assignment of the Size-dependent Optical Spectrum in CdSe Quantum Dots. *Phys. Rev. B* **1996**, *53*, 16338–16346.
37. Chen, O.; Yang, Y.; Wang, T.; Wu, H.; Niu, C.; Yang, J.; Cao, Y. C. Surface-Functionalization-Dependent Optical Properties of II-VI Semiconductor Nanocrystals. *J. Am. Chem. Soc.* **2011**, *133*, 17504–17512.
38. To probe the robustness of this result we also performed simulations reducing artificially the conduction band offset at the CdSe/CdS heterojunction to 0.1 eV (see supporting information). The calculated spectra did not reveal qualitative differences despite the enhanced asymmetry of the electron wave functions.
39. Hens, Z.; Moreels, I. Light Absorption by Colloidal Semiconductor Quantum Dots. *J. Mater. Chem.* **2012**, *22*, 10406.
40. Ninomiya, S.; Adachi, S. Optical Properties of Cubic and Hexagonal CdSe. *J. Appl. Phys.* **1995**, *78*, 4681–4689.

41. Ninomiya, S.; Adachi, S. Optical Properties of Wurtzite CdS. *J. Appl. Phys.* **1995**, *78*, 1183–1190.
42. Xu, C.; Webb, W. W. Measurement of Two-photon Excitation Cross Sections of Molecular Fluorophores with Data from 690 to 1050 Nm. *J. Opt. Soc. Am. B* **1996**, *13*, 481–491.
43. Configuration-interaction calculations of the lowest-lying excitonic states were also conducted to probe the influence of the Coulomb energy and electron-hole correlations on the predicted blue shifts (see supporting information). No noticeable changes arose with respect to the single particle model.
44. Rajadell, F.; Climente, J. I.; Planelles, J.; Bertoni, A. Excitons, Biexcitons, and Trions in CdSe Nanorods. *J. Phys. Chem. C* **2009**, *113*, 11268–11272.
45. Laheld, U. E. H.; Einevoll, G. T. Excitons in CdSe Quantum Dots. *Phys. Rev. B* **1997**, *55*, 5184–5204.
46. Button, K. J.; Lax, B.; Cohn, D. R. Piezoelectric Polaron-Cyclotron Resonance in the Quantum Limit in n-CdS. *Phys. Rev. Lett.* **1970**, *24*, 375–378.
47. Sitt, A.; Della Sala, F.; Menagen, G.; Banin, U. Multiexciton Engineering in Seeded Core/Shell Nanorods: Transfer from Type-I to Quasi-type-II Regimes. *Nano Lett.* **2009**, *9*, 3470–3476.

TOC GRAPHIC

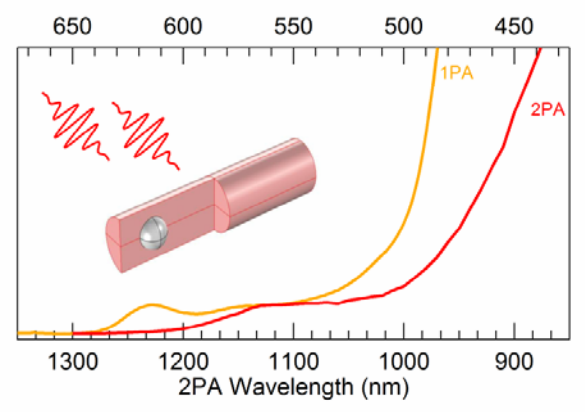
650
600
550
500
450
1PA
2PA
1300
1200
1100
1000
900
2PA Wavelength (nm)